

THE ORBITS OF NEPTUNE’S OUTER SATELLITES

MARINA BROZOVIĆ¹, ROBERT A. JACOBSON¹, AND SCOTT S. SHEPPARD²

¹ Jet Propulsion Laboratory, California Institute of Technology, 4800 Oak Grove Drive, Pasadena, CA 91109-8099, USA;
marina.brozovic@jpl.nasa.gov, raj@jpl.nasa.gov

² Carnegie Institution of Washington, Department of Terrestrial Magnetism, 5241 Broad Branch Road NW, Washington, DC 20015, USA; sheppard@dtm.ciw.edu
Received 2010 October 27; accepted 2011 February 7; published 2011 March 10

ABSTRACT

In 2009, we used the Subaru telescope to observe all the faint irregular satellites of Neptune for the first time since 2004. These observations extend the data arcs for Halimede, Psamathe, Sao, Laomedeia, and Neso from a few years to nearly a decade. We also report on a search for unknown Neptune satellites in a half-square degree of sky and a limiting magnitude of 26.2 in the R band. No new satellites of Neptune were found. We numerically integrate the orbits for the five irregulars and summarize the results of the orbital fits in terms of the state vectors, post-fit residuals, and mean orbital elements. Sao and Neso are confirmed to be Kozai librators, while Psamathe is a “reverse circulator.” Halimede and Laomedeia do not seem to experience any strong resonant effects.

Key words: astrometry – celestial mechanics – ephemerides – planets and satellites: general – planets and satellites: individual (Neptune)

Online-only material: extended figure

1. INTRODUCTION

A planet’s gravity dominates the dynamical orbital evolution of the satellites that reside within its Hill sphere. The mean radius of a Hill sphere is estimated (for a circular approximation of the planet’s orbit) as $R_H = a_p(\mu/3)^{1/3}$, where a_p is the semimajor axis of the planet’s heliocentric orbit and $\mu = m_p/(m_p + m_{\text{Sun}})$ is the ratio of the planet’s and Sun’s masses. The outer planets have a number of satellites within their Hill spheres. The satellites closest to the planet are called the “regulars,” and it is generally thought that they formed at the same time as the planet itself. They are characterized by almost circular orbits that lie near the equatorial plane of the planet. They also orbit in the same direction as the planet orbits about the Sun (so-called direct orbits). Further away from the planet, a dynamically diverse population of satellites with potentially various origins is encountered. They are called the “irregulars” and are characterized by their distant orbits with large inclinations, eccentricities, and long periods that may take decades to complete. Neptune’s irregular satellite population has orbital properties similar to those of the irregular satellites of Jupiter, Saturn, and Uranus (Gladman et al. 1998; Jewitt & Haghighipour 2007; Nicholson et al. 2008). There are many theories on how the outer planets acquired their outer satellites. As an ice giant, Neptune most likely did not have dissipative gas drag captures (Saha & Tremaine 1993; Gladman et al. 2001; Brunini et al. 2002), but it could have acquired some of its irregulars via collisional capture (Colombo & Franklin 1971), or chaos assisted capture from low-energy orbits (Astakhov et al. 2003), or various binary capture scenarios (Agnor & Hamilton 2006; Nesvorný et al. 2007; Vokrouhlický et al. 2008; Gaspar et al. 2010; Philpott et al. 2010).

There are two very distinct odd-balls among Neptune’s satellites: Nereid and Triton. Triton is a giant the size of Pluto, and it orbits Neptune in an almost circular, but retrograde orbit. Nereid is thought to be a regular moon of Neptune that was ejected into the outer satellites’ realm during the gravitational capture of Triton (Goldreich et al. 1989). Nereid revolves around Neptune in a highly eccentric (0.75), direct orbit with a low

inclination, and an orbital period just short of one Earth year (360 days). The most current orbital fits for Triton and Nereid have been discussed in Jacobson (2009).

In this paper, we present orbital fits and report on the new measurements for the five recently discovered outermost Neptunian irregulars: Halimede (S/2002 N1), Sao (S/2002 N2), Laomedeia (S/2002 N3), Neso (S/2002 N4), and Psamathe (S/2003 N1). The first four satellites were discovered by Holman et al. (2004) during their 2002 survey when they covered approximately 1.4 deg² around Neptune and had 50% detection efficiency for $m_R \sim 25.5$ objects. Sheppard et al. (2006) surveyed approximately 1.75 deg² around Neptune in August of 2003 with an estimated detection efficiency of 50% for $m_R \sim 25.8$. This corresponds to a survey of satellites with radii greater than 17 km, assuming an optical albedo of 0.04. This search uncovered a fifth satellite—Psamathe. In retrospect, Holman et al. (2004) also registered Psamathe on a single night in 2001. Two of the irregulars (Sao and Laomedeia) are in direct orbits and three (Halimede, Psamathe, and Neso) are in retrograde orbits.

2. METHODS

2.1. Orbital Model

The orbits were obtained via numerical integration of the equations of motion (Peters 1981). We used a variable order Gauss–Jackson integration method with an average step size of 32,000 s. The equations are formulated in the Cartesian coordinate system with the Neptunian system barycenter at the origin. The model’s coordinate frame is referenced to the International Celestial Reference Frame. We used barycentric dynamical time (TDB); TDB is the standard relativistic coordinate time in JPL’s planetary and satellite ephemerides.

Our model of the outer satellite orbits takes into account the equatorial bulge of Neptune and perturbations from external bodies as well as perturbations from Triton. All of our previous analyses (Jacobson 1990, 2009; Jacobson et al. 1991) treated Nereid as massless, and we retain this assumption. The external perturbations include Jupiter, Saturn, Uranus, and the Sun with

Table 1
Dynamical Constants Used in the Orbit Integration

Name	Value
Neptune system GM ($\text{km}^3 \text{s}^{-2}$) ^a ..	6836527.1006
Triton GM ($\text{km}^3 \text{s}^{-2}$) ^a	1427.5981
Jovian system GM ($\text{km}^3 \text{s}^{-2}$) ^b	126712764.8000
Saturnian system GM ($\text{km}^3 \text{s}^{-2}$) ^c	37940585.2000
Uranian system GM ($\text{km}^3 \text{s}^{-2}$) ^d ..	5794557.0000
Sun GM ($\text{km}^3 \text{s}^{-2}$) ^b	132713233263.2381
Neptune radius (km) ^a	25225.0
Neptune J_2 ^a	3.408×10^{-3}
Neptune J_4 ^a	-3.340×10^{-5}
Neptune pole R.A. ^a (deg).....	299.461
Neptune pole decl. ^a (deg).....	43.405

Notes.^a Jacobson (2009).^b Folkner et al. (2008), Sun GM augmented with the masses of the inner planets.^c Jacobson et al. (2006).^d Jacobson (2007).**Table 2**
Halimede (S/2002 N1) Observations

Year	Observatory	Data Points	References
1999	568 Mauna Kea/CFHT	3	MPC 49878 ^a
2001	807 Cerro Tololo obs./La Serena	3	MPC 47500
2002	807 Cerro Tololo obs./La Serena	6	MPC 47500
2002	309 Cerro Paranal	8	MPC 47500
2003	304 Las Campanas obs.	8	MPC 49423
2003	807 Cerro Tololo obs./La Serena	6	MPC 49423
2003	568 Mauna Kea/Subaru	5	MPC 49423
2003	304 Las Campanas obs.	3	MPC 49767
2004	568 Mauna Kea/CFHT	3	MPC 52492
2004	304 Las Campanas obs.	3	MPC 52312
2004	568 Mauna Kea/CFHT	2	MPC 54697
2009	568 Mauna Kea/Subaru	8	This paper

Note. ^a Pre-discovery.

its mass augmented by the masses of the inner planets. JPL ephemeris DE421 (Folkner et al. 2008) provides the positions of the major planets and the Sun while the perturbative effects of Triton are included based on the NEP081 (Jacobson 2009) ephemeris file.

The complete list of dynamical constants necessary for integration is shown in Table 1. The parameters listed are GMs associated with the various perturbative sources as well as the J_2 and J_4 coefficients that define the effects of an oblate Neptune. The outer satellites are small, and their GMs are unknown so for modeling purposes they are considered massless.

2.2. Observations

The observations used in this analysis are listed in Tables 2–6. The data are shown individually for each satellite with the number of data points per year and per observatory. The majority of the data are publicly available via Minor Planet Circulars (MPCs). We report the 2009 measurements in Table 7 in the format (1/100 of an arcsec precision) as they would be reported to the Minor Planet Center. However, the astrometry is only good to around a few tenths of an arcsecond.

We used the Subaru 8.2 m telescope with the wide-field Suprime-Cam imager to recover the known Neptune satellites and to survey the space around Neptune for possible additional

Table 3
Psamathe (S/2003 N1) Observations

Year	Observatory	Data Points	References
2001	807 Cerro Tololo obs./La Serena	3	MPC 49423
2002	807 Cerro Tololo obs./La Serena	4	MPC 49423
2003	807 Cerro Tololo obs./La Serena	9	MPC 49423
2003	568 Mauna Kea/Subaru	5	MPC 49423
2004	568 Mauna Kea/CFHT	2	MPC 54697
2004	304 Las Campanas obs.	3	MPC 52313
2004	568 Mauna Kea/CFHT	2	MPC 52492
2009	568 Mauna Kea/Subaru	8	This paper

Table 4
Sao (S/2002 N2) Observations

Year	Observatory	Data Points	References
2001	568 Mauna Kea/CFHT	3	MPC 47500
2002	807 Cerro Tololo obs./La Serena	6	MPC 47500
2002	309 Cerro Paranal	14	MPC 47501
2003	807 Cerro Tololo obs./La Serena	2	MPC 49767
2003	568 Mauna Kea/Subaru	5	MPC 49767
2004	568 Mauna Kea/CFHT	2	MPC 52492
2004	304 Las Campanas obs.	2	MPC 52312
2004	568 Mauna Kea/CFHT	4	MPC 54697
2004	309 Cerro Paranal	2	MPC 54697
2009	568 Mauna Kea/Subaru	5	This paper

Table 5
Laomedeia (S/2002 N3) Observations

Year	Observatory	Data Points	References
2001	807 Cerro Tololo obs./La Serena	3	MPC 47501
2002	807 Cerro Tololo obs./La Serena	6	MPC 47501
2002	309 Cerro Paranal	8	MPC 47501
2003	568 Mauna Kea/Subaru	4	MPC 49767
2003	304 Las Campanas obs.	3	MPC 49767
2004	304 Las Campanas obs.	7	MPC 52313
2004	568 Mauna Kea/CFHT	2	MPC 54697
2009	568 Mauna Kea/Subaru	5	This paper

Table 6
Neso (S/2002 N4) Observations

Year	Observatory	Data Points	References
2002	807 Cerro Tololo obs./La Serena	6	MPC 49767
2002	309 Cerro Paranal	6	MPC 49767
2002	950 La Palma	3	MPC 49767
2003	807 Cerro Tololo obs./La Serena	4	MPC 49767
2003	304 Las Campanas obs.	7	MPC 49767
2004	568 Mauna Kea/CFHT	2	MPC 54697
2004	304 Las Campanas obs.	3	MPC 52313
2004	568 Mauna Kea/CFHT	2	MPC 52492
2009	568 Mauna Kea/Subaru	5	This paper

satellites. Suprime-Cam has 10 2048×4096 CCDs arranged in a 5×2 pattern (Miyazaki et al. 2002) with $15\mu\text{m}$ pixels that give a scale of $0''.20 \text{ pixel}^{-1}$. This gives a field of view of about $34' \times 27'$ with the north–south direction along the long axis. There are gaps between the chips of about $16''$ in the north–south direction and only $3''$ in the east–west direction.

Images were obtained on the (UT) nights of 2009 June 21 and 22 and October 14 and 15. The very wide VR broadband filter covering the usual Johnson–Kron–Cousins V and R bands was used with the telescope autoguided sidereally. Image reduction was performed by first bias-subtracting and then flat-fielding

Table 7
2009 Mauna Kea/Subaru Observations of Neptune’s Irregular Satellites

Object	Date ^a	R.A.	Decl.	Mag./Filter
Halimede	2009 06 22.57094	21 53 28.295	-13 21 30.27	<i>R</i>
Halimede	2009 06 22.58758	21 53 28.241	-13 21 30.32	<i>R</i>
Halimede	2009 06 22.60438	21 53 28.187	-13 21 30.69	<i>R</i>
Halimede	2009 10 14.20981	21 43 38.251	-14 10 05.99	24.7 <i>R</i>
Halimede	2009 10 14.23858	21 43 38.165	-14 10 06.39	<i>R</i>
Halimede	2009 10 14.25350	21 43 38.125	-14 10 06.56	<i>R</i>
Halimede	2009 10 15.25694	21 43 35.440	-14 10 17.97	<i>R</i>
Halimede	2009 10 15.27153	21 43 35.400	-14 10 18.32	<i>R</i>
Psamathe	2009 06 22.57094	21 52 36.926	-12 55 13.24	<i>R</i>
Psamathe	2009 06 22.58758	21 52 36.898	-12 55 13.45	<i>R</i>
Psamathe	2009 06 22.60438	21 52 36.829	-12 55 13.68	<i>R</i>
Psamathe	2009 10 14.20981	21 42 55.760	-13 45 21.23	25.6 <i>R</i>
Psamathe	2009 10 14.23858	21 42 55.688	-13 45 21.63	<i>R</i>
Psamathe	2009 10 14.25350	21 42 55.638	-13 45 21.84	<i>R</i>
Psamathe	2009 10 15.25694	21 42 53.035	-13 45 35.32	<i>R</i>
Psamathe	2009 10 15.27153	21 42 53.006	-13 45 35.71	<i>R</i>
Sao	2009 10 14.20981	21 43 22.894	-14 06 02.33	25.8 <i>R</i>
Sao	2009 10 14.23858	21 43 22.807	-14 06 02.74	<i>R</i>
Sao	2009 10 14.25350	21 43 22.775	-14 06 03.11	<i>R</i>
Sao	2009 10 15.25694	21 43 20.208	-14 06 17.98	<i>R</i>
Sao	2009 10 15.27153	21 43 20.165	-14 06 18.17	<i>R</i>
Laomedeia	2009 10 14.21725	21 46 02.914	-14 03 30.39	25.3 <i>R</i>
Laomedeia	2009 10 14.24606	21 46 02.820	-14 03 30.82	<i>R</i>
Laomedeia	2009 10 14.26093	21 46 02.777	-14 03 31.00	<i>R</i>
Laomedeia	2009 10 15.26389	21 46 00.113	-14 03 43.29	<i>R</i>
Laomedeia	2009 10 15.27917	21 46 00.102	-14 03 43.73	<i>R</i>
Neso	2009 10 14.21725	21 45 32.911	-13 52 45.68	25.2 <i>R</i>
Neso	2009 10 14.24606	21 45 32.814	-13 52 46.03	<i>R</i>
Neso	2009 10 14.26093	21 45 32.771	-13 52 46.35	<i>R</i>
Neso	2009 10 15.26389	21 45 29.930	-13 52 59.16	<i>R</i>
Neso	2009 10 15.27917	21 45 29.887	-13 52 59.49	<i>R</i>

Note. ^a Times are given for the middle of the observations.

with twilight flats. Seeing (measured as the width of a Gaussian that matches the point-source profile) on the nights of June 22 and October 14 and 15 was very good, around 0.5 arcsec. Seeing on June 21 was not as good, around 0.8 arcsec. Neptune was not near opposition during these observations since these images were acquired at the very beginning or end of the nights while searching for Neptune Trojans 60° ahead and behind the planet (Sheppard & Trujillo 2010). Neptune and any outer satellites were thus only moving about -1.8 arcsec hr⁻¹ in right ascension (R.A.) and -0.7 arcsec hr⁻¹ in declination (decl.) in the June fields and -1.6 and -0.5 arcsec hr⁻¹ in the October fields. Because of the slower movement individual image exposures could be longer than possible when Neptune is near opposition since trailing loss is less of a factor. Individual exposures were 600–700 s each.

Because of the large field of view of the Suprime-Cam, all six known (Nereid included) outer satellites of Neptune could be imaged on just two Suprime-Cam fields. We thus oriented two Suprime-Cam fields in order to recover all known outer satellites of Neptune. The images were visually blinked in order to recover the known satellites and search for new satellites of Neptune. All six known outer irregular satellites were easily recovered without knowing their precise positions within the two fields (Figure 1). Because the fields were off opposition, foreground asteroids and background Kuiper Belt Objects could mimic the motion of a Neptune satellite over a few hours. These objects were easily discarded when comparing the consecutive nights of October 14 and 15 since any object not near Neptune would have

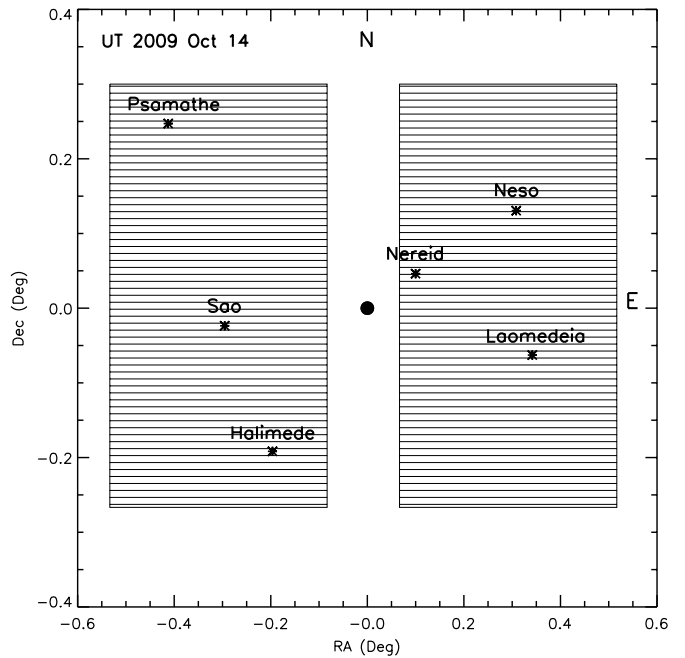


Figure 1. Area imaged around Neptune for satellites using the Suprime-Cam on the 8.2 m Subaru telescope. The black dot at the center represents Neptune’s position. Stars represent the positions of the outer satellites of Neptune. All six known outer satellites of Neptune could be recovered in just two fields with Suprime-Cam.

movement that was not uniform and consistent like the Neptune satellites over a 24 hr period. Because of the superior seeing on consecutive nights in October, these images were the primary ones used in our attempt to discover possible new satellites.

By placing artificial objects matched to the point-spread function of the images, we found that the 50% limiting magnitude of the images was at an *R*-band magnitude of 26.2 (Figure 2). This is several tenths of a magnitude fainter than any previous survey for satellites around Neptune (Holman et al. 2004; Sheppard et al. 2006). We did not find any new Neptune satellite candidates in our two fields. Though the two fields only cover about 0.51 deg² of Neptune’s 3.5 deg² inner Hill sphere, these fields contained all of the known Neptune outer satellites that had not been observed since 2004. It is thus likely that any unknown satellites would be in these fields as well. In addition, Neptune is the only planet that has not yet had its inner 70% Hill sphere completely searched with modern CCD detectors, which means relatively bright satellites could easily have been missed in previous searches.

2.3. Data Weights

We used the same reasoning regarding the data weights as in our previous paper (Brozovic & Jacobson 2009). All results presented in this paper (e.g., state vectors, residuals, mean orbital elements) are based on weighting the data set uniformly at 1 arcsec. This perhaps does not utilize the measurements to their maximum potential (many measurements have accuracies far better than 1 arcsec), but we felt that this is a more conservative approach to obtaining the baseline results. However, we do use the inverse of the root-mean-square (rms) weighting procedure to obtain an alternative orbital fit. The difference between the alternate orbit and our baseline orbit provides one measure of the orbit uncertainty.

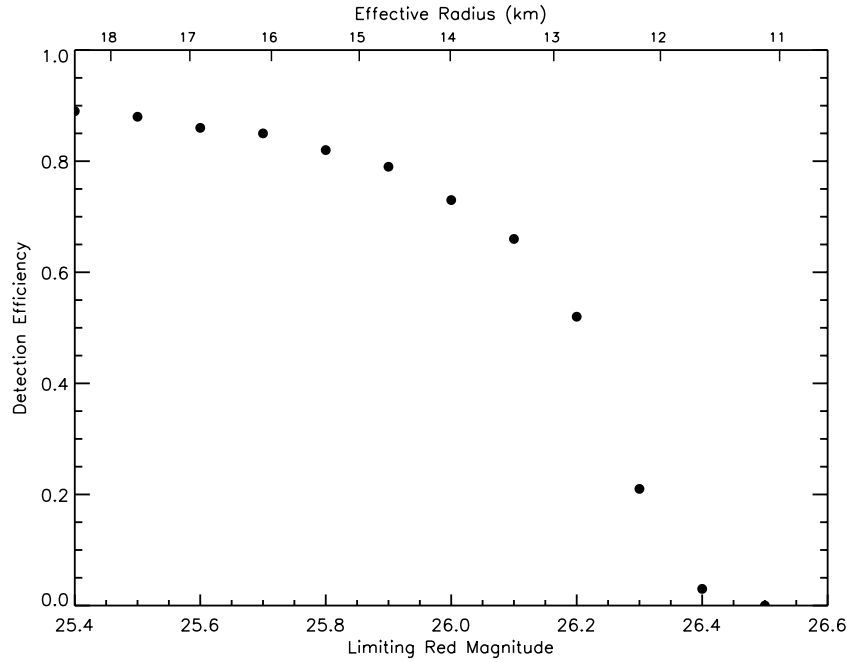


Figure 2. Detection efficiency of the Neptune satellite survey vs. apparent red magnitude. The 50% detection efficiency is at an R band of about 26.2 mag as determined by visual blinking of fields with implanted artificial moving objects at Neptune satellite apparent velocities. Effective radii of the apparent magnitude were calculated assuming an albedo of 0.05.

Table 8
Epoch for State Vectors is 1999 January 22 TDB

Satellite	Position (km)	Velocity (km s ⁻¹)
Halimede	-11293356.94703422	-0.3247130566545486
	-8624555.365297209	-0.2033011672702937
	-15151383.58790347	-0.3150438399272822
Psamathe	44720975.90590505	0.1318196515007334
	17976669.81962686	-0.2306067610259427
	-39975630.38711110	0.0198644063804478
Sao	4037451.905241752	-0.4316913323806180
	14013321.40488383	-0.2782477085832223
	13102663.29469588	0.3557825625416940
Laomedeia	21103905.10871873	0.2847818213269017
	-2278189.032865756	0.2940849712360937
	-20279742.74257871	0.0889952126457492
Neso	-50082036.01780124	0.1616907100266050
	57806647.98898701	0.0835483566125447
	-28419675.49966229	0.0402928414700149

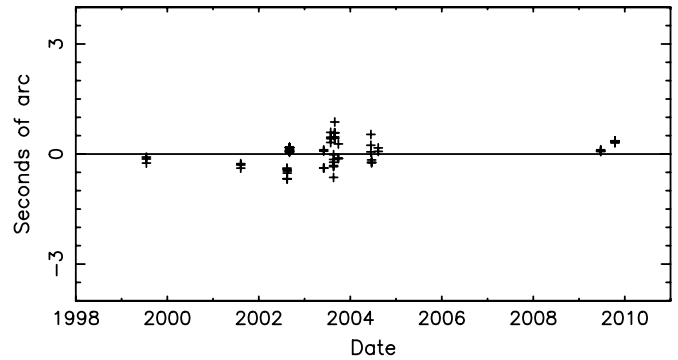


Figure 3. Halimede right ascension residuals.

Table 9
Observation Residual Statistics

Satellite	No.	R.A. (arcsec)	Decl. (arcsec)
Halimede	58	0.351	0.428
Psamathe	36	0.395	0.614
Sao	45	0.417	0.474
Laomedeia	38	0.165	0.284
Neso	38	0.400	0.541

3. RESULTS

3.1. Epoch State Vectors and Residuals

The epoch state vectors of the integrated orbits were found by a least-squares fit (Lawson & Hanson 1974) to the observations. The values listed in Table 8 have a precision of nine decimal places in order to allow for the future orbit integrations. The epoch for all state vectors is 1999 January 22 TDB.

Table 9 shows the post-fit observation residual statistics (R.A. and decl.) for each satellite. The residuals reflect the accuracy of the orbital fits, and the average rms of 0.5 arcsec is a typical value of an orbital fit to a dim, distant object (e.g., outer Jovian satellites, outer Uranian satellites, Saturnian moon Phoebe). Figures 3 through 12 show the distribution of the individual data point residuals for each satellite. Most of these residuals lie well within the 1 arcsec limit which implies that the orbital solution represents the current set of measurements well. However, we

have to keep in mind that the data sets are very sparse. As an example, Psamathe and Neso have orbital periods of ~ 25 and ~ 27 yr, and they were discovered less than a decade ago. Thus, we only have data arcs that extend over less than half of their orbits.

3.2. Accuracy of the Orbital Fits

Orbital uncertainties are always challenging to estimate and one has to carefully investigate if the numbers are overly optimistic or pessimistic. We can obtain a measure of an uncertainty by mapping the orbital covariance over time. This

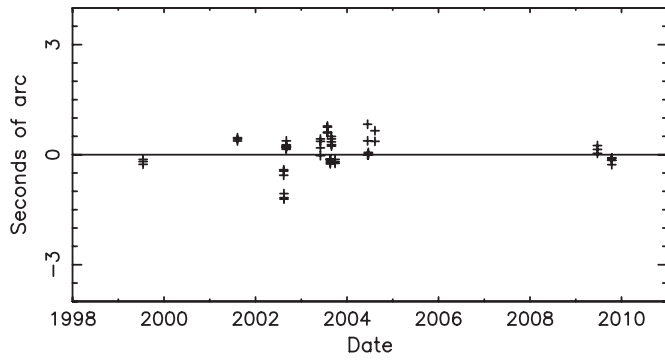


Figure 4. Halimede declination residuals.

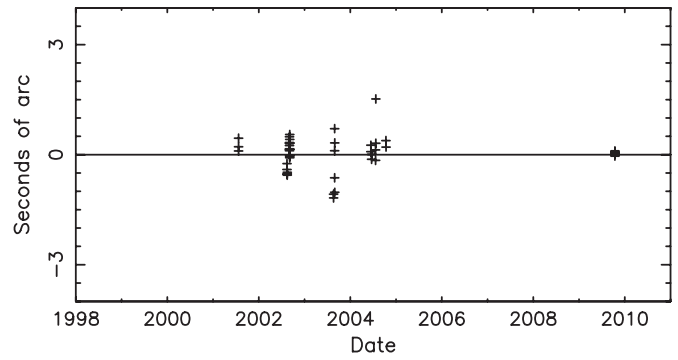


Figure 8. Sao declination residuals.

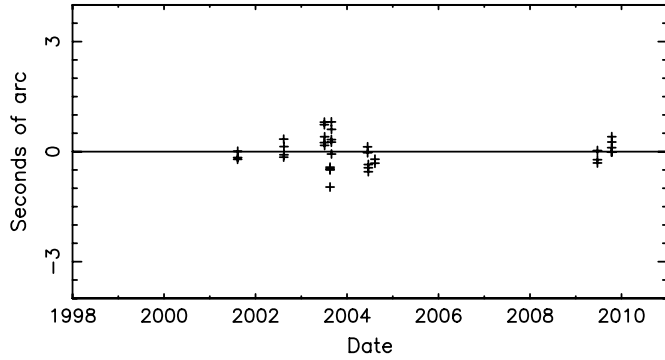


Figure 5. Psamathe right ascension residuals.

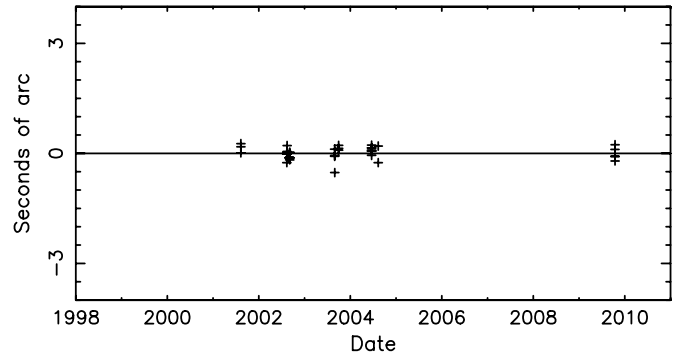


Figure 9. Laomedea right ascension residuals.

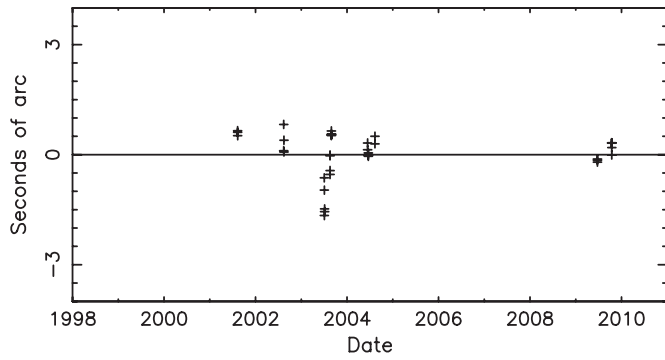


Figure 6. Psamathe declination residuals.

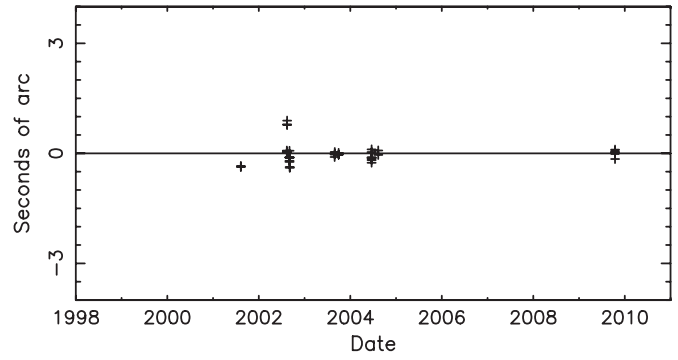


Figure 10. Laomedea declination residuals.

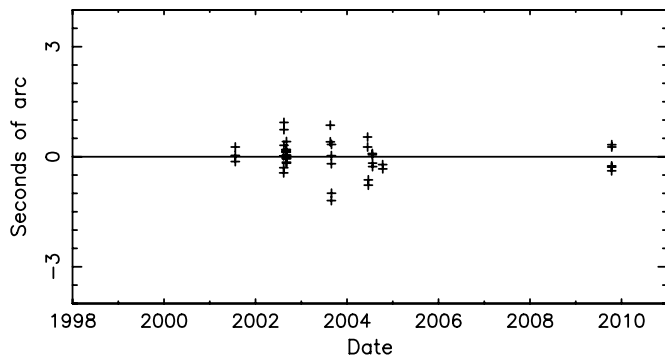


Figure 7. Sao right ascension residuals.

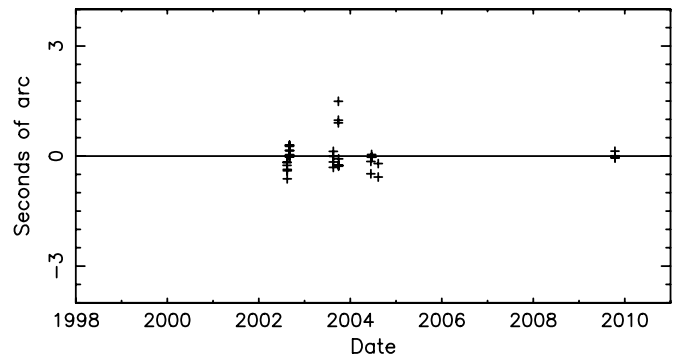


Figure 11. Neso right ascension residuals.

method is equivalent to a Monte Carlo method assuming Gaussian noise statistics (a reasonable assumption in the absence of a direct knowledge of the actual statistics of our error sources).

It is important to note that covariance mapping may produce artificially small uncertainties unless we have highly accurate observations in combination with a very detailed model that in-

cludes higher order effects. This can be overcome by introducing un-modeled sources of errors as either non-updating parameters or “consider” parameters (Jacobson 2009). For example, in our baseline model, we assumed that Neptune’s position was known. In an extension of the baseline model, we include Neptune’s astrometry data set and solve for the orbital parameters of

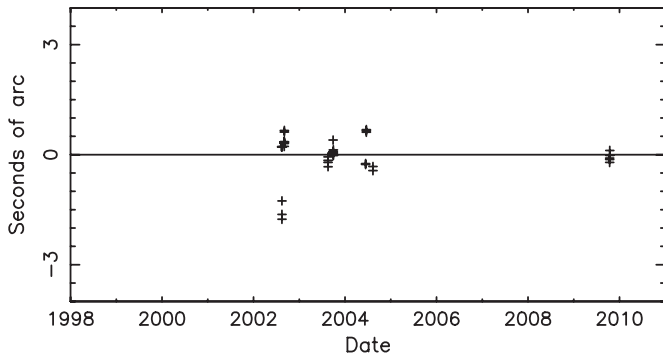


Figure 12. Neso declination residuals.

Table 10
Mapped Covariance (B-baseline Model, E-extended Model) Over
One, Three, and Ten Orbital Periods for Each Satellite

Satellite	σ_1 (arcsec)		σ_3 (arcsec)		σ_{10} (arcsec)	
	B	E	B	E	B	E
Halimede	1	2	2	4	6	11
Psamathe	35	37	78	84	320	340
Sao	2	4	3	6	9	17
Laomedeia	3	4	7	12	20	33
Neso	170	190	400	430	790	890

Notes. The numbers have been rounded to two significant digits. At Neptune, 1 arcsec is equal to 21,063 km.

Neptune. This procedure allows the uncertainty in the Neptune orbit, as determined by the Neptune astrometry, to influence the uncertainties in the satellite orbit. As another example of extending the sources of uncertainties, we added in our “consider” list biases (such as R.A. and decl. astrometry biases of 200 mas) that represent errors in the star catalogs. These considered parameters have their values and uncertainties assigned as “a priori” values and we did not solve for them in our model. Their primary role is to inflate the statistics of the resulting orbital fit.

We mapped the covariances of both the baseline model as well as the extended (added sources of the uncertainties) orbital model over a duration of one, three, and ten orbital periods for each of the satellites (Table 10). This progressively longer mapping gives an idea of error growth. The mapped covariances for the extended model are always greater than the covariances for the baseline model, which proves that our method for producing more conservative errors worked. Psamathe and Neso have particularly high uncertainties because their data arcs cover less than one orbital period.

As a second test of our orbital fit accuracy, we used the difference between the orbital fits between our baseline and extended models. Figures 13 and 14 show the plane-of-sky difference in the orbital position as predicted by two fits. Psamathe’s differences are mapped over 250 years and Neso’s over 270 years. The differences start small, but they grow in time as we depart from the data arc. It is also important to note that the uncertainties depend on where in the orbit (geometrically) we are trying to assess the satellite position. When compared with Table 10, we see that the differences stay well below the covariances and we take this as a good sign that we have a conservative estimate for the uncertainties.

In our previous paper (Brozovic & Jacobson 2009), we used the difference between rms weighted and uniformly weighted

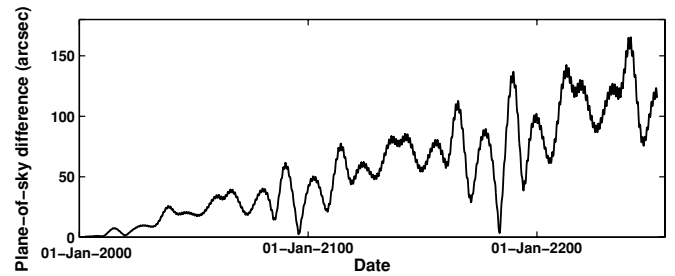


Figure 13. Psamathe plane-of-sky differences between the baseline orbital solution and the extended orbital solution used to produce inflated mapped covariance.

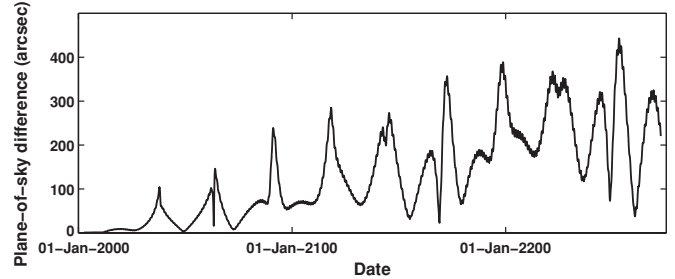


Figure 14. Neso plane-of-sky differences between the baseline orbital solution and the extended orbital solution used to produce inflated mapped covariance.

data (our baseline model) as a measure of the orbital uncertainty. We tested this method on the current data set and found that it produced the least conservative uncertainties.

3.3. Long-term Orbital Integration and Mean Orbital Elements

We fitted a precessing ellipse to a 6000 year orbital integration and summarized this fit by a set of mean elements. The extra long integration assures that the mean elements are not affected by any long-term orbital perturbations. In order to pursue such a long integration, we needed the planetary ephemerides that provide the positions of the planets over this integration period (JPL’s DE408 ephemerides; E. M. Standish 2005, private communication) as well as a 6000 year ephemeris file for the perturbing Triton (Jacobson 2009). We note that our data arcs cover less than half of the orbital paths for Psamathe and Neso which may, as a consequence, produce integrated orbital fits that differ from reality. Thus, the derived mean elements could be far from the truth despite capturing the integrated orbital fit in its essence. It is likely that our estimates for periods of periapsis and node contain large errors because our data are certainly not strong enough to constrain these periods over thousands of years.

The mean orbital elements for the 6000 year integration are shown in Table 11. The reference plane for all satellites is set to the ecliptic plane. The epoch for the orbital elements is 2000 January 1 TDB. The parameters listed in the tables are a is the semimajor axis, e is the eccentricity, I is the inclination, λ is the mean longitude, ϖ is the periapsis longitude, Ω is the longitude of the ascending node, $d\lambda/dt$ is the mean longitude rate, $d\varpi/dt$ is the periapsis rate, and $d\Omega/dt$ is the nodal rate.

Kozai (1962) first showed that the precession of the argument of perihelion stops at large inclinations in the asteroid belt ($d\omega/dt = d\varpi/dt - d\Omega/dt \approx 0$). A similar condition has been proven for the irregular satellites of the outer planets (Carruba et al. 2002; Nesvorný et al. 2003). Satellites that are in Kozai resonance have an argument of pericenter ω librating about 90° or 270° , while the eccentricity and inclination endure coupled

Table 11
Planetocentric Mean Orbital Elements in Ecliptic Coordinates

Element	Halimede	Psamathe	Sao	Laomedeia	Neso
a (km)	16681000	46705000	22619000	23613000	50258000
e	0.29	0.46	0.28	0.43	0.42
I (deg)	112.90	137.68	49.91	34.05	131.27
λ (deg)	169.49	346.58	138.65	342.71	252.18
ϖ (deg)	304.68	206.19	125.63	199.05	38.37
Ω (deg)	217.22	297.13	60.58	59.50	48.02
$d\lambda/dt$ (deg day ⁻¹)	0.1916	0.0394	0.1233	0.1134	0.0364
$d\varpi/dt$ (deg century ⁻¹)	4.40	-3.23	-6.77	5.21	-31.40
$d\Omega/dt$ (deg century ⁻¹)	1.95	27.59	-6.69	-10.83	32.90

Note. The epoch for the orbital elements is 2000 January 1 TDB.

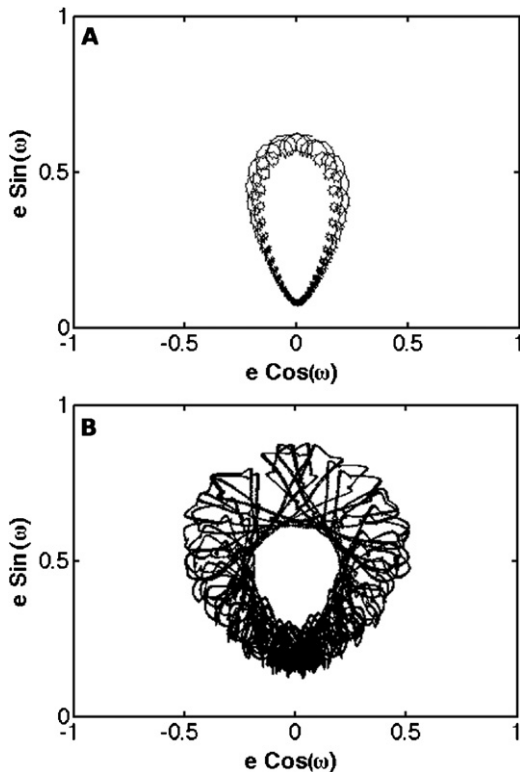


Figure 15. Kozai dynamics of (A) direct Sao and (B) retrograde Neso during the 6000 years long integration in $(e \cos(\omega), e \sin(\omega))$ phase space.

oscillations. Holman et al. (2004) and Ćuk & Burns (2004) suggested that Sao (direct) could be in a Kozai resonance. Ćuk & Burns (2004) suggested that Neso (retrograde) too could be a Kozai liblator.

We confirm that both irregulars have an argument of pericenter librating of about 90° . Sao has a relatively small amplitude of osculating inclination (40° – 55°) while its eccentricity changes from 0.07 to 0.63. For direct Sao, the highest eccentricity corresponds to the smallest inclination. Neso has a much more extreme orbit with an osculating inclination in the range 117° – 146° and an eccentricity that oscillates from 0.13 to 0.88. For retrograde Neso, the maximum inclination corresponds to the maximum eccentricity. Figure 15 displays Kozai dynamics in terms of $e \cos(\omega)$ and $e \sin(\omega)$ as in Thomas & Morbidelli (1996) and Nesvorný et al. (2003). If we compare our results to the theoretical curves based on the Kozai Hamiltonian (Figure 7 in Nesvorný et al. 2003), we see that our osculating elements capture many higher order effects over 6000 years. We

can also say that, on average, the analytical model is an excellent approximation. The main source of wiggles and complex patterns in Figure 15 is most likely the tidal forcing from the Sun. As a first-order estimate, the solar perturbation strength can be computed as $(a/R_H)^3$, where a is the satellite’s orbital semimajor axis and R_H is the Hill radius for Neptune ($R_H = 0.775$ AU). For direct Sao, the solar perturbation’s strength is 0.007, and for retrograde Neso it is more than 10 times stronger at 0.082. For comparison, retrograde Jovians experience solar tugs on the order 0.064–0.097 (Carruba et al. 2002). We have directly investigated the influence of solar perturbations on the orbital paths of Sao and Neso by removing Jupiter, Saturn, Uranus, and Triton from our numerical integration and leaving only the Sun as the perturber. The orbital paths over the 6000 integration in Figure 15 remained virtually unchanged. Thus, we conclude that the Sun must be the primary source of the perturbations.

Figure 16 shows another example of interesting dynamics among Neptune’s irregulars. Again, similar to the dynamical trajectories predicted by the Kozai Hamiltonian in Figure 7 in Nesvorný et al. (2003), we find that Halimede and Psamathe do not move on ω librating trajectories but on ω circulating trajectories. More precisely, Halimede and Psamathe follow a “figure eight” path just outside the separatrices of the libration island in $e \cos(\omega)$ and $e \sin(\omega)$ phase space. Halimede has a very high inclination (111° – 144°) paired with an eccentricity in the range of 0.19–0.90. Similarly, Psamathe has an inclination in the range 117° – 148° and an eccentricity varying from 0.07 to 0.88. It is interesting to note that Psamathe experiences almost as strong solar perturbations as Neso ($(a/R_H)^3 = 0.065$); this is evident in the complex variability of its path in Figure 16.

Ćuk & Burns (2004) suggested that both Psamathe and Halimede could be “reverse circulators.” These are the objects occupying the region between the secular ($d\varpi/dt - d\varpi_{\text{planet}}/dt \approx 0$) and Kozai resonances. A reverse circulator has a period for the argument of pericenter circulation longer than the period of node circulation, which results in the precession of ϖ being dominated by the nodal rate and always in the opposite direction from the orbital motion. Our latest orbital elements confirm that Psamathe is indeed a reverse circulator, but Halimede is not. Halimede still has ϖ circulating regularly in the direction of its orbital motion.

Finally, Laomedeia has the least extreme orbit of Neptune’s five irregulars discussed here. This satellite shows only very modest oscillations in inclination (30° – 43°) and eccentricity (0.29–0.56) while the argument of pericenter circulates very uniformly over 360° .

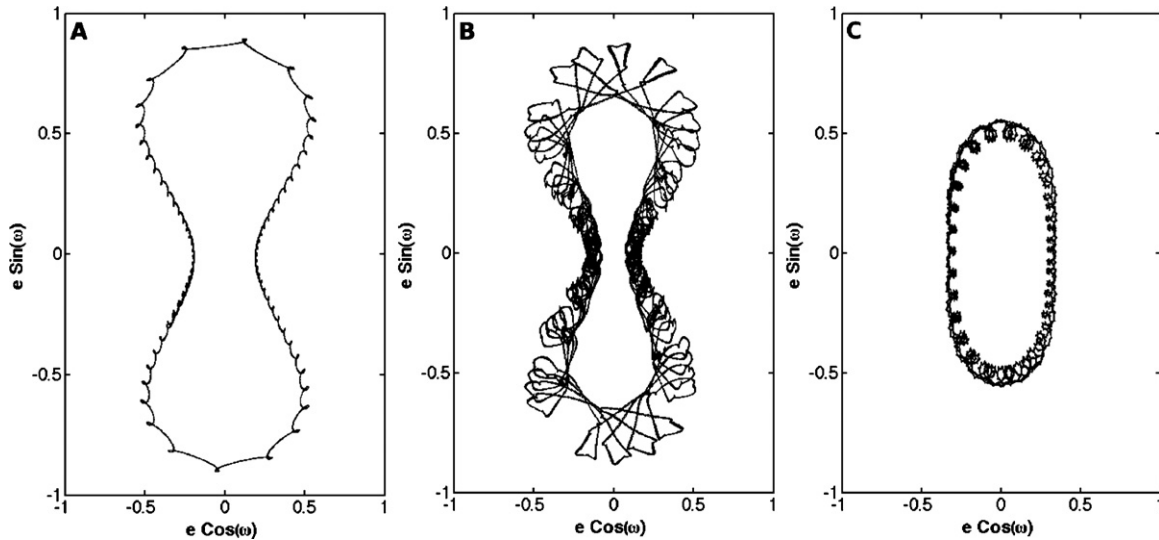


Figure 16. Circulating trajectories of (A) retrograde Halimede, (B) retrograde Psamathe, and (C) direct Laomedea during the 6000 years long integration in $(e \cos(\omega), e \sin(\omega))$ phase space.

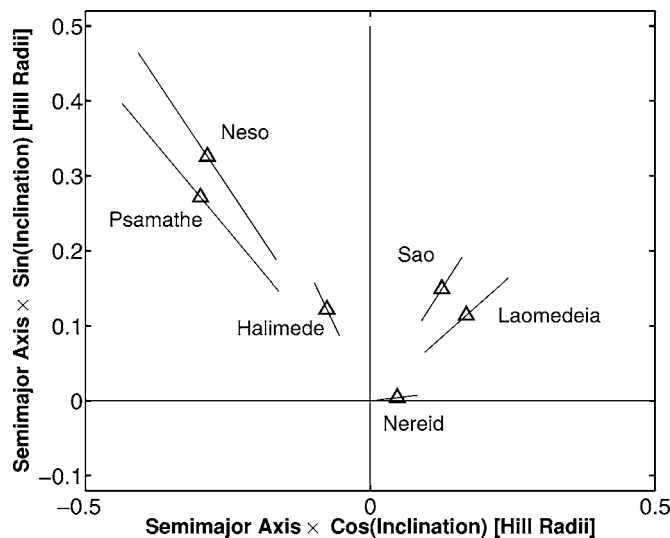


Figure 17. Spatial distribution for the irregular satellites of Neptune. (An extended version of this figure is available in the online journal.)

4. DISCUSSION

Our analysis is an extension of R. A. Jacobson’s (2008, unpublished) orbital calculations for the Neptunian irregulars, which was posted as NEP078 on JPL’s Horizons online solar system data and ephemeris computation service (Giorgini et al. 1996). Our results incorporate the latest measurements from 2009.

We summarize the spatial distribution (in Hill radii) of five Neptunian irregulars in Figure 17 (an extended version of this figure can be found in the online journal). We also added Nereid based on the mean elements (converted to the ecliptic coordinates) published in Jacobson (2009). The lines represent the mean pericenter-to-apocenter variation due to the orbital eccentricity for each of the satellites.

Psamathe and Neso are two retrogrades that have similar orbital elements and thus may have a common origin in a once-larger parent (Holman et al. 2004; Sheppard et al. 2006). The third retrograde, Halimede, has a similar average inclination (113°) but otherwise different orbital elements than the other

two. As suggested by Holman et al. (2004), Halimede could still have a common origin with Psamathe and Neso if the “chaos assisted capture” is invoked. Briefly, Astakhov et al. (2003) proposed that the giant planets might have captured objects in low-energy heliocentric orbits via an “intermediate” chaotic stage which allowed just enough time for some other mechanism (e.g., gas drag) to place the object in a planetocentric stable orbit. Objects that would have been captured in such circumstances would keep the common “inclination memory” while the other orbital elements would freely disperse. As an alternative theory, Halimede could share its origin with Nereid. Holman et al. (2004) found that there is 0.41 probability of a collision between Halimede and Nereid over 4.5 Gyr, which also suggests that Halimede could be a collisional fragment of Nereid.

We have shown that Sao and Neso are both Kozai librators while Psamathe experiences some resonant effects. The Kozai resonance has proven to be an important orbit altering mechanism that can bring an outer satellite within the reach of the massive regular satellites, or even the planet, or alternatively, it can take it outside the Hill sphere and thus free it from planetocentric orbit. As a direct consequence of the Kozai resonance, very few satellites have orbits with an inclination with respect to the ecliptic (or planet’s heliocentric orbital plane) between 50° and 140° (Carruba et al. 2002; Nesvorný et al. 2003). In their study of stable/unstable orbits, Nesvorný et al. (2003) found that instabilities due to Kozai resonances occur in a narrower inclination range ($80 \lesssim i \lesssim 100$ for $e = 0$ and/or $\omega = 90^\circ$) for Neptune than for Jupiter or Saturn. This is a direct consequence of Triton being very close to the planet ($a_T = 0.00236$ AU) so it is harder for it to collide with the Kozai bound irregular. Also, many highly eccentric satellite orbits are long lived because of the small value of Triton’s semimajor axis. Nesvorný et al. (2003) concluded that the orbital configuration of the massive inner satellites directly influences the size of the Kozai resonance zone.

5. CONCLUDING REMARKS

We report on 2009 optical observations with the Subaru telescope for the five outermost Neptunian irregulars. We found no new Neptune satellites to a limiting R -band magnitude of 26.2, which is several tenths of a magnitude fainter than any of

the previous surveys (Holman et al. 2004; Sheppard et al. 2006). We have integrated the equations of motion that model the orbital trajectories for the satellites. The least-squares procedure was used to fit the free parameters in the model to the set of Earth-based measurements from 1999 to 2009. We have shown that Neptunian irregulars represent a diverse dynamical system with two Kozai librators and one reverse circulator. We would like to reiterate the importance of new measurements, especially for the cases of Psamathe and Neso because of their long orbital periods. Their orbits contain large uncertainties and any new measurements would reduce the risk of losing these objects in the future. Ephemerides (NEP085) based on the orbits described in this paper are available electronically from the JPL Ephemeris Horizons Web site (<http://ssd.jpl.nasa.gov/horizons.cgi>).

The research described here was carried out at the Jet Propulsion Laboratory, California Institute of Technology, under contract with the National Aeronautics and Space Administration. This manuscript was based partially on data collected at the Subaru telescope, which is operated by the National Astronomical Observatory of Japan. The authors thank all of the astronomers who contributed to these orbital calculations with their measurements.

REFERENCES

- Agnor, C. B., & Hamilton, D. P. 2006, *Nature*, **441**, 192
- Astakhov, S. A., Burbanks, A. D., Wiggins, S., & Farrelly, D. 2003, *Nature*, **423**, 264
- Brozovic, M., & Jacobson, R. A. 2009, *AJ*, **137**, 3834
- Brunini, A., Parisi, M. G., & Tancredi, G. 2002, *Icarus*, **159**, 166
- Carruba, V., Burns, J. A., Nicholson, P. D., & Gladman, B. J. 2002, *Icarus*, **158**, 434
- Colombo, G., & Franklin, F. A. 1971, *Icarus*, **15**, 186
- Ćuk, M., & Burns, J. A. 2004, *AJ*, **128**, 2518
- Folkner, W. M., Williams, J. G., & Boggs, D. H. 2008, The Planetary and Lunar Ephemeris DE421, Interoffice Memo. 343R-08-003 (Internal Document; Pasadena, CA: Jet Propulsion Laboratory)
- Gaspar, H. S., Winter, O. C., & Viera Neto, E. 2010, arXiv:1002.2392v1
- Giorgini, J. D., et al. 1996, *BAAS*, **28**, 1158
- Gladman, B. J., Nicholson, P. D., Burns, J. A., Kavelaars, J. J., Marsden, B. G., Williams, G. V., & Offutt, W. B. 1998, *Nature*, **392**, 897
- Gladman, B. J., et al. 2001, *Nature*, **412**, 163
- Goldreich, P., Murray, N., Longaretti, P. Y., & Banfield, D. 1989, *Science*, **245**, 500
- Holman, M. J., et al. 2004, *Nature*, **430**, 865
- Jacobson, R. A. 1990, *A&A*, **231**, 241
- Jacobson, R. A. 2007, *BAAS*, **39**, 453
- Jacobson, R. A. 2009, *AJ*, **137**, 4322
- Jacobson, R. A., Riedel, J. E., & Taylor, A. H. 1991, *A&A*, **247**, 565
- Jacobson, R. A., Spitale, J., Porco, C. C., & Owen, W. M., Jr. 2006, *AJ*, **132**, 711
- Jewitt, D., & Haghighipour, N. 2007, *ARA&A*, **45**, 261
- Kozai, Y. 1962, *AJ*, **67**, 591
- Lawson, C. L., & Hanson, R. J. 1974, Solving Least Squares Problems (Englewood Cliffs, NJ: Prentice-Hall, Inc.)
- Miyazaki, S., et al. 2002, *PASJ*, **54**, 833
- Nesvorný, D., Alvarillos, J. L. A., Dones, L., & Levison, H. F. 2003, *AJ*, **126**, 398
- Nesvorný, D., Vokrouhlický, D., & Morbidelli, A. 2007, *AJ*, **133**, 1962
- Nicholson, P., Ćuk, M., Sheppard, S., Nesvorný, D., & Johnson, T. 2008, in The Solar System Beyond Neptune, ed. M. A. Barucci, H. Boehnhardt, D. P. Cruikshank, & A. Morbidelli (Tucson, AZ: Univ. Arizona Press), 441
- Peters, C. F. 1981, *A&A*, **104**, 37
- Philpott, C. M., Hamilton, D. P., & Agnor, C. B. 2010, *Icarus*, **208**, 824
- Saha, P., & Tremaine, S. 1993, *Icarus*, **106**, 549
- Sheppard, S. S., Jewitt, D. J., & Kleyna, J. 2006, *AJ*, **132**, 171
- Sheppard, S. S., & Trujillo, C. A. 2010, *Science*, **329**, 1304
- Thomas, F., & Morbidelli, A. 1996, *Celest. Mech. Dyn. Astron.*, **64**, 209
- Vokrouhlický, D., Nesvorný, D., & Levison, H. F. 2008, *AJ*, **136**, 1463